RESEARCH ARTICLE

JENER Journal of Empirical and Non-Empirical Research
Volume 2, Issue 5, Page 438-446 | Article No. 52
DOI: 10.4898/jener.v2i5.a52
ISSN: 7895-9216
Journal homepage: https://jenerjournal.com
Journal email: editor@jenerjournal.com

JENER Journal
JENER Journal of Empirical and Non-Empirical Research

Influence of Nonlinear Elastic Foundation Models on the Optimal Design of Steel Rectangular Liquid-Storage Tanks: Winkler, Kondner Hyperbolic, and Polynomial Subgrade Representations

Ali H. Ajaam[1]

[1]Faculty of Engineering\ Almusayib, University of Babylon, Babylon, Iraq

ARTICLE INFORMATION

Article history:
Published: May 2026

Keywords:
Steel Rectangular Tank
Nonlinear Elastic Foundation
Soil-Structure Interaction
Structural Optimization
Elastic-Plastic FEM

ABSTRACT

This paper investigates the influence of three elastic foundation models on the optimal design of steel rectangular liquid-storage tanks: the linear Winkler model, the Kondner hyperbolic model, and a polynomial subgrade model. An elastic-plastic incremental finite element analysis is developed using eight-node serendipity flat shell elements based on Mindlin thick-plate theory, with the von Mises yield criterion expressed in terms of stress resultants and the Prandtl-Reuss flow rule governing material nonlinearity. Soil-structure interaction is incorporated through nonlinear normal subgrade reaction stiffness matrices, derived from the secant modulus of each foundation model, coupled with a linear Winkler horizontal subgrade reaction. A modified Hooke and Jeeves direct-search algorithm performs constrained nonlinear optimization to minimize total shell material volume for a specified liquid storage capacity while satisfying geometric and plastic-design constraints. Parametric studies on open-topped and closed rectangular steel tanks resting on dense sand and loose sand show that the square plan shape consistently yields the minimum-volume design, that the optimal width-to-depth ratio is approximately 3:1, and that the optimal shell volume and dimension ratios are remarkably insensitive to the choice of foundation model. The total shell volume differs by less than 4% between the two polynomial soil models examined. These findings justify the use of simpler linear Winkler models in preliminary optimization, while recommending nonlinear models for detailed floor slab thickness determination under soft soil conditions.

1. Introduction

Steel rectangular tanks are widely employed in municipal water supply, industrial process facilities, and petroleum storage. Because these structures are repetitive by nature, even modest reductions in shell material volume accumulate into substantial cost savings across large infrastructure programs. Accurate structural analysis coupled with systematic optimization therefore has considerable practical significance [1]. The structural behaviour of such tanks is governed by three interacting phenomena: the elastic and post-yield response of the steel shell under hydrostatic loading; the resistance provided by the supporting soil; and the coupled deformation field arising from their interaction. Classical analyses assume linear elastic material response and idealize the foundation as a bed of independent linear Winkler springs [2]. While computationally tractable, this idealization does not reproduce the nonlinear load-settlement characteristics consistently observed in field plate-load tests [3,4] and confirmed by recent soil-structure interaction studies [5,6].

Growing recognition of soil nonlinearity has motivated increasingly sophisticated foundation models. The hyperbolic law proposed by Kondner [7] for triaxial compression has been extended to the plate-load test setting to yield a nonlinear secant modulus that decreases with settlement [8]. Polynomial regression of experimental data provides an alternative capable of capturing both stiffening and softening trends [9]. Despite the availability of these models, their quantitative influence on the optimal design of steel tanks has not been systematically examined.

On the structural side, adoption of elastic-plastic finite element methods for thin-walled shells has demonstrated that purely elastic designs are inherently conservative, because post-yield stress redistribution provides additional load-carrying capacity [10,11]. Recent coupled soil-structure-interaction studies on dynamic loading of rectangular tanks [12,13] and liquid natural gas vessels [14] further highlight the inadequacy of decoupled elastic analyses. For steel tanks under static hydrostatic loading, the combination of material nonlinearity and foundation nonlinearity within a single optimization framework remains unexplored in the open literature. The present paper addresses this gap using the computer program OPTANK, developed from incremental elastic-plastic plate analysis [15], extended to nonlinear folded-plate structures [16] and elastic foundations [9]. Three objectives are pursued:

- To formulate and validate an elastic-plastic incremental FEM for rectangular steel tanks resting on nonlinear elastic foundations, incorporating three alternative subgrade reaction laws.
- To integrate the structural analysis with a modified Hooke and Jeeves constrained optimization algorithm minimizing total shell material volume.

- To quantify the sensitivity of the optimal design—dimensions, thickness ratios, and shell volume—to the choice of foundation model across dense sand and loose sand conditions.

2. Background and Literature Review

2.1 Analysis of rectangular liquid-storage tanks

Early analytical work on rectangular tank behaviour relied on finite-difference plate solutions [17], moment-distribution procedures [18], and space-frame analogies [19]. The finite element method was applied to tanks on elastic springs by Cheung and Zienkiewicz [1] in 1965 and extended to three-dimensional rectangular tank analysis by Cheung and Davies [2,20]. These studies confirmed the importance of wall-floor-roof interaction and showed that one-dimensional bending assumptions underestimate corner moments. Uraiby [21] implemented nine-node Lagrangian shell elements for reinforced concrete rectangular tanks on Winkler foundations, and Karkush [16] developed an incremental finite-strip formulation for elastic-perfectly-plastic folded steel structures.

Recent developments in the field have strengthened both the analysis and the optimization of tank structures. Vestergaard et al. [22] proposed a stress-based shell element using convex optimization for efficient elastic-plastic limit-state analysis, demonstrating that models with over 10,000 elements can be solved within minutes on standard hardware. Truong and Chou [23] integrated enhanced metaheuristic search with nonlinear FEA to minimize the weight of multi-member steel structures, while Ghaemifard and Ghannadiasl [24] confirmed through a comparative study of eleven algorithms that direct-search methods remain competitive for constrained structural problems when paired with FEA. For large petroleum storage tanks, Zhao et al. [25] used the Ramberg-Osgood nonlinear material model to show that foundation settlement conditions significantly govern wall deformations and that plastic material models are essential for realistic assessments.

2.2 Optimal design of tanks

Structural optimization of liquid-storage tanks has been pursued almost exclusively for reinforced concrete designs. Meichoers and Rozvany [26] minimized reinforcing steel volume in circular tanks using lower-bound plastic analysis. Adidam and Subramanyam [27] applied constrained nonlinear programming to cylindrical RC tank walls. Abdul-Hussain [28] studied underground RC rectangular tanks and found that the square plan shape minimizes material volume. Therendran and Thambiratnam [29] minimized cylindrical tank wall thickness by coupling FEM with Rosenbrock optimization. Al-Ne'aimi and Al-Sabah [30,31] incorporated Winkler soil-structure interaction in the minimum-cost design of cylindrical tanks, showing that soil stiffness significantly affects optimal geometry. To the authors' knowledge, no previous published work has coupled elastic-plastic FEA of steel rectangular tanks with nonlinear subgrade models within a systematic optimization framework.

2.3 Soil foundation models and soil-structure interaction

The Winkler model represents soil as independent linear springs with constant modulus k_z [kN/m³]. Loukidis and Tamiolakis [32] showed that a uniform modulus of subgrade reaction significantly underestimates mat-foundation bending moments compared to a continuum model, emphasizing the importance of appropriate spring stiffness distribution even within the linear framework.

Kondner [7] proposed the hyperbolic stress-strain law for soils, subsequently adapted to plate-load tests as $P = \delta/(a + b\delta)$ [8]. Mourya et al. [5] reviewed continuum, Winkler-based, and macroelement models for soil-structure-foundation interaction, concluding that nonlinear Winkler springs represent an effective balance between accuracy and computational cost for practical engineering analyses.

Recent studies on the seismic response of rectangular liquid-storage tanks have demonstrated that SSI effects are significant. Kumar and Saha [13] found that the effectiveness of isolation systems depends strongly on soil type and tank slenderness. Rawat et al. [12] employed fully coupled Eulerian-Lagrangian FEA to show that ignoring SSI can yield unrealistic predictions of tank performance. Jing et al. [33] further showed that structure-soil-structure interaction between adjacent tanks modifies their seismic response. Although these studies address dynamic loading, the interaction mechanisms they identify inform the static problem addressed here.

3. Finite Element Formulation

3.1 Flat shell element

The structural shell is discretized using eight-node serendipity flat shell elements, each a superposition of a Mindlin thick-plate bending element and a plane-stress membrane element. The element provides five degrees of freedom per node: transverse displacement w, mid-surface in-plane displacements u and v, and average rotations θ_x and θ_y. A sixth drilling rotation θ_z is appended to couple elements lying in non-coplanar planes [10].

The Mindlin formulation assumes: (i) deflection w is small; (ii) normals to the mid-surface remain straight but not necessarily normal after deformation; and (iii) the transverse normal stress σ_z is negligible. Transverse shear strains are corrected by $\kappa^2 = 5/6$ to produce a parabolic cross-sectional distribution consistent with cross-sectional warping.

The displacement field within each element is interpolated using the eight-node serendipity shape functions $N_i(\zeta, \eta)$:

$$\{u\} = [N]\{d\} \quad (1)$$

where {d} is the vector of nodal degrees of freedom and [N] is the shape function matrix. The same functions map the physical coordinates:

$$x = \Sigma N_i x_i, \quad y = \Sigma N_i y_i \quad (2)$$

The transformation from physical (x, y) to isoparametric (ζ, η) coordinates is carried out through the Jacobian matrix:

$$[J] = \begin{bmatrix} \partial x/\partial\zeta & \partial y/\partial\zeta \\ \partial x/\partial\eta & \partial y/\partial\eta \end{bmatrix} \quad (3)$$

The strain-displacement matrix [B] is obtained by differentiating Eq. (1) with respect to physical coordinates using $[J]^{-1}$, leading to the element stiffness integral:

$$[K_e] = \iint [B]^T [D_{ep}] [B] |J| \, d\zeta \, d\eta \quad (4)$$

where $[D_{ep}]$ is the elastic or elastic-plastic constitutive matrix and $|J|$ is the Jacobian determinant. Numerical integration uses a full 3×3 Gauss rule for bending and membrane terms and a reduced 2×2 rule for transverse shear terms to prevent shear locking. Integration through the thickness employs six Gauss points.

3.2 Elastic-plastic constitutive relations

An elastic-perfectly-plastic material model is adopted. Yielding initiates when the effective stress $\bar{\sigma}$ exceeds the uniaxial yield stress σ_y. For a general stress state the von Mises criterion in stress space is:

$$\bar{\sigma} = [\sigma_x^2 - \sigma_x \sigma_y + \sigma_y^2 + 3\tau_{xy}^2 + 3\tau_{xz}^2 + 3\tau_{yz}^2]^{1/2} \leq \sigma_y \quad (5)$$

For the flat shell element under plane-stress conditions ($\sigma_z \approx 0$), Eq. (5) reduces to:

$$\bar{\sigma} = [\sigma_x^2 - \sigma_x \sigma_y + \sigma_y^2 + 3\tau_{xy}^2]^{1/2} \leq \sigma_y \quad (6)$$

For the plate-bending formulation, the von Mises criterion is expressed in terms of equivalent bending moments through standard stress-resultant transformation relations [10,36]. Integrating the stress distribution through the thickness for a rectangular section at the plastic limit, the yield criterion takes the form:

$$f = M_x^2 - M_x M_y + M_y^2 + M_{xy}^2 - M_p^2 \leq 0 \quad (7)$$

where $M_p = \sigma_y t^2/4$ is the full plastic moment per unit width for a rectangular cross-section of thickness t. This expression is the moment-space equivalent of the von Mises criterion and is consistent with the approach of Owen and Hinton [10] and Save and Massonnet [36].

When membrane force resultants N_x, N_y are significant (as in the tank walls), the reduced plastic moment M_p^* under combined bending and axial action is approximated by the standard interaction relation [37]:

$$M_p^* = M_p [1 - (N / N_p)^2] \quad (8)$$

where N is the in-plane force resultant and $N_p = \sigma_y t$ is the squash load per unit width [37]. Equation (8) ensures that cross-sections carrying significant axial force have appropriately reduced plastic moment capacity.

The incremental plastic strain vector is related to the yield-function gradient through the Prandtl-Reuss flow rule:

$$\{d\varepsilon_p\} = d\lambda \, \{\partial f/\partial \sigma\} \quad (9)$$

where $d\lambda \geq 0$ is an instantaneous proportionality constant. Enforcing consistency on the yield surface yields the elastic-plastic constitutive matrix:

$$[D_{ep}] = [D_e] - [D_e]\{a\}\{a\}^T [D_e] / (\{a\}^T [D_e]\{a\} + H') \quad (10)$$

where $\{a\} = \partial f/\partial \sigma$ and $H' = 0$ for elastic-perfectly-plastic behaviour.

3.3 Nonlinear foundation stiffness matrices

The base slab of the tank rests on the soil. Following the approach of Al-Khafaji [9], the soil is modelled through a foundation stiffness matrix assembled from nodal spring constants. The continuous foundation stiffness matrix at element level is:

$$[K_f]^e = \int_A [N]^T [k_s] [N] \, dA \quad (11)$$

where $[k_s] = \mathrm{diag}(k_z, k_x, k_y)$ contains the normal and tangential subgrade moduli at each point on the base slab. In the discrete finite element implementation, the nodal normal spring constant K_z for node i is the secant subgrade modulus evaluated at the current nodal settlement δ_i, multiplied by the tributary area:

$$K_z(i) = k_z(\delta_i) \times \alpha_i h^2 \quad (12)$$

where h is the element mesh dimension and $\alpha_i = 1/8$ at corner nodes and 2/8 at mid-side nodes. Three laws for the normal secant modulus $k_z(\delta)$ are employed:

- Winkler (linear): $k_z = k_s$ = constant. This is the baseline model with no settlement dependence [1,2,32].
- Kondner hyperbolic: $P = \delta/(a + b\delta)$, giving $k_z = dP/d\delta = a/(a + b\delta)^2$. Parameters a (mm³/kN) and b (mm²/kN) are determined from the transformed δ/P vs. δ plot of plate-load test data, where a is the intercept and b is the slope [7,8].
- Polynomial: $P = \Sigma c_j \delta^j$, giving $k_z = \Sigma j c_j \delta^{(j-1)}$. Coefficients are obtained by least-squares regression of experimental plate-load test data [9].

Horizontal subgrade resistance (base-slab friction) is represented by linear Winkler springs with constant moduli k_x and k_y throughout.

3.4 Three-level incremental solution algorithm

A three-level iterative procedure governs the nonlinear solution: subincrements nested within modified Newton-Raphson iterations, which are nested within load increments. The key steps are:

- At the start of each load increment i, the element stiffness matrices are updated using $[D_{ep}]$ evaluated at the current stress state at each Gauss point, then assembled into the global stiffness matrix $[K]_i$. This matrix is held constant for all iterations within that increment.
- At each Newton-Raphson iteration j, the displacement increment $\{\delta u\}_j$ is computed from the residual force vector. Element strain increments and an effective elastic-plastic strain increment are evaluated at each Gauss point.
- The effective strain increment at each Gauss point is subdivided into subincrements of size limited to the criterion: $d\varepsilon_{ep}^{(m)} \leq 0.0002$, consistent with recommended values for ductile metallic materials [10]. For each subincrement m, the stress increment is computed from Eq. (10), accumulated, and scaled back onto the yield surface to eliminate numerical drift.
- Convergence within each load increment is assessed by the residual-force norm. The analysis terminates when this norm falls below 10% of the applied load norm (convergence), or when it increases between successive iterations (structural collapse, signalling the collapse load factor).

4. Optimization Formulation

The design variables are the plan length L, width W, depth D, floor thickness t_f, wall thicknesses t_l and t_w (x- and y-directions), and, for closed tanks, roof thickness t_r. The objective function is total shell material volume V:

$V = L \cdot W \cdot t\_f + 2(L \cdot D \cdot t\_l) + 2(W \cdot D \cdot t\_w)$ [$+ L \cdot W \cdot t\_r$ for closed tanks] (13)

Constraints are: $L > 0$, $W > 0$, $D \geq D\_min$ (functional minimum depth), and the plastic-design yield constraint derived from Eqs. (7) and (8). This constraint ensures that the specified collapse load factor λ_c is attained without any cross-section becoming fully plastic through its thickness at the design load level.

The modified Hooke and Jeeves direct-search method [34] navigates the design space through alternating exploratory moves—systematic perturbation of each design variable by step h_j—and pattern moves along the direction established by recent successful explorations. Constraints are enforced by assigning a large penalty value whenever a trial point violates any geometric or yield constraint, redirecting the search into the feasible region. The method requires only function evaluations rather than gradients, making it well suited to problems where each evaluation involves a complete nonlinear structural analysis [24]. Numerical experiments found that a step length of 0.1 to 0.2 times the smallest design variable provides satisfactory convergence.

5. Validation of the Finite Element Formulation

The accuracy and robustness of the developed elastic-plastic finite element formulation were verified through comparison with six independent benchmark problems from the literature. The examples cover elastic and elastic-plastic plate bending, hydrostatic loading of shell walls, folded-plate structures, open and closed rectangular tanks, and tanks on elastic foundations. In all examples the present formulation employed eight-node serendipity flat-shell elements with selective reduced integration. Convergence studies were conducted for each example to identify the minimum mesh density required for stable and accurate results.

5.1 Simply supported elastic-plastic square plate

Geometry and material properties: Plate span: L = 1.0 m; thickness: t = 0.01 m, Young's modulus: E = 10.92 MN/m²; Poisson's ratio: ν = 0.30, Yield stress: σ_y = 1600 MN/m². Owing to symmetry, one quarter of the plate was modelled, Figure 1(a). A mesh convergence study using 1, 4, and 9 eight-node shell elements over the quarter model confirmed that a 2×2 mesh (4 elements) provides satisfactory convergence with minimal computational cost. The load increment after first yield was set to $\Delta\lambda = \lambda\_y / 20$, where λ_y is the first-yield load factor.

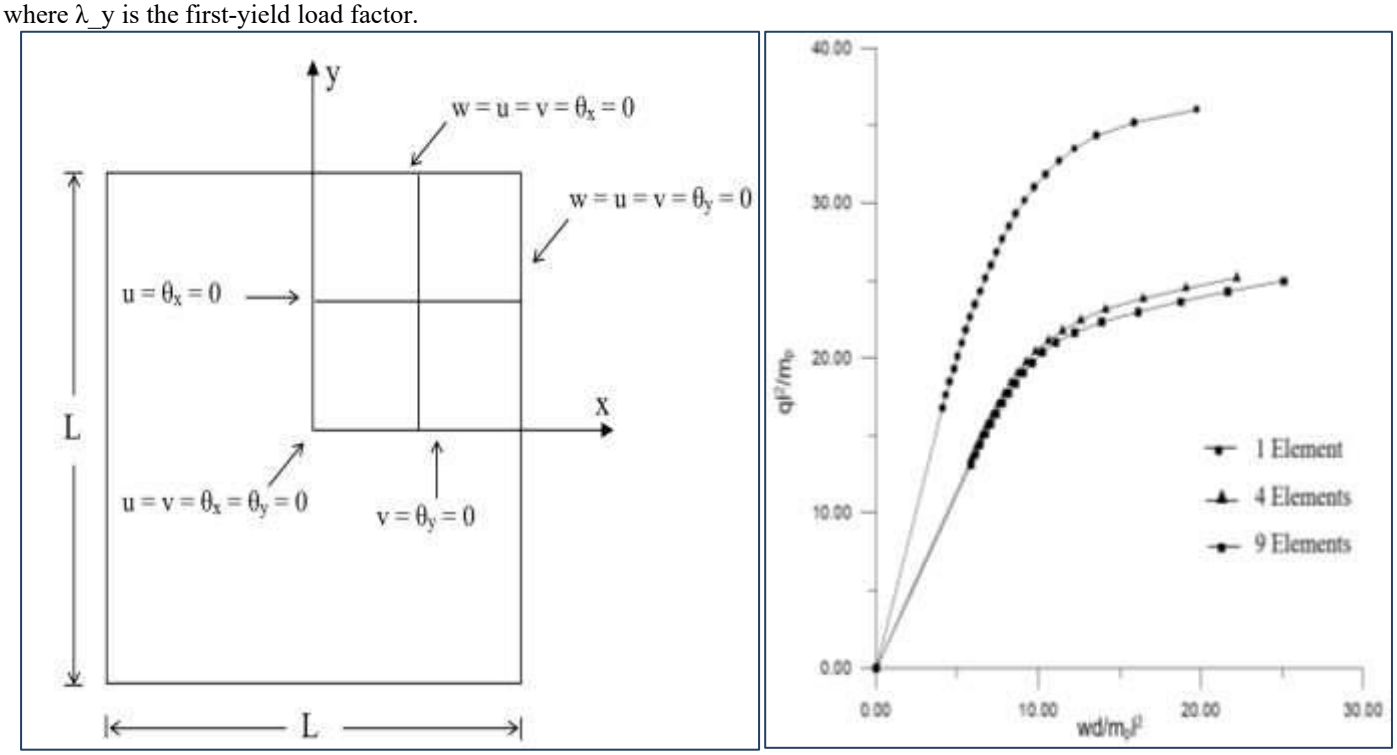

Figure 1: (a) Simply supported square plate, (b) Load verses central deflection for different mesh sizes

The computed load-deflection response at the plate centre closely matches the benchmark solution of Hinton and Owen [10]. The difference in collapse load was only 0.17% and the corresponding central deflection differed by 0.63%, as shown in Figure 1 (b). These results confirm that the present incremental elastic-plastic formulation accurately captures stiffness degradation and post-yield redistribution in plate bending.

5.2 Rectangular wall subjected to hydrostatic pressure

Wall properties: Length = 6.0 m; Width = 10.0 m; Thickness = 0.20 m, Maximum hydrostatic pressure: q_0 = 60 kN/m², Young's modulus: E = 2×10^7 kN/m²; Poisson's ratio: ν = 1/6, Boundary conditions: three built-in edges, one free edge.Due to symmetry, one-half of the wall was discretized using a 5×5 finite element mesh, Figure 2. Computed bending moments were compared with the classical analytical solution of Timoshenko and Woinowsky-Krieger [35] and the FEM results of Uraiby [21]. Results are summarized in Table 1.

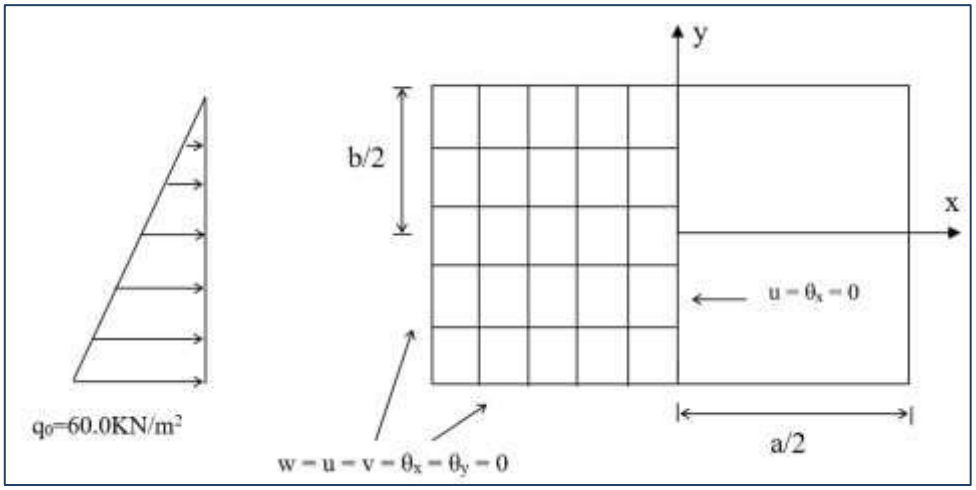

Figure 2: Rectangular wall with hydrostatic pressure

Table 1. Bending moments (N·m/m) in a rectangular wall under hydrostatic pressure.

Method	M_x at x=0, y=b/2	M_x at x=a/2, y=b/2	M_y at x=0, y=−b/2
Timoshenko [35]	53.4	−107.7	−145.2
Uraiby [21]	51.9	−103.4	−140.4
Present study	47.3	−101.1	−139.0

The mean deviation from Timoshenko's solution is 7.9% and from Uraiby's FEM is 4.3%. The improved agreement with Uraiby is attributed to the similarity of formulation; the residual difference reflects the use of eight-node versus nine-node elements.

5.3 Simply supported elastic-plastic box beam.

Material and geometric properties: Span length: L = 6.0 m, Young's modulus: E = 210 GPa; Yield stress: σ_y = 240 MPa; Poisson's ratio: ν = 0.0. One quarter of the beam was modelled using four shell elements. The mid-span load-deflection response was compared with ADINA results reported by Ng et al. [11] and with Karkush's incremental finite-strip solution [16], as shown is figure 3 (a). Differences in collapse load were 2.29% relative to ADINA and 0.76% relative to Karkush; corresponding displacement differences were approximately 10% and 6%, respectively, see Figure 3 (b). The close agreement confirms the capability of the formulation to model progressive plastic redistribution in folded-plate steel structures.

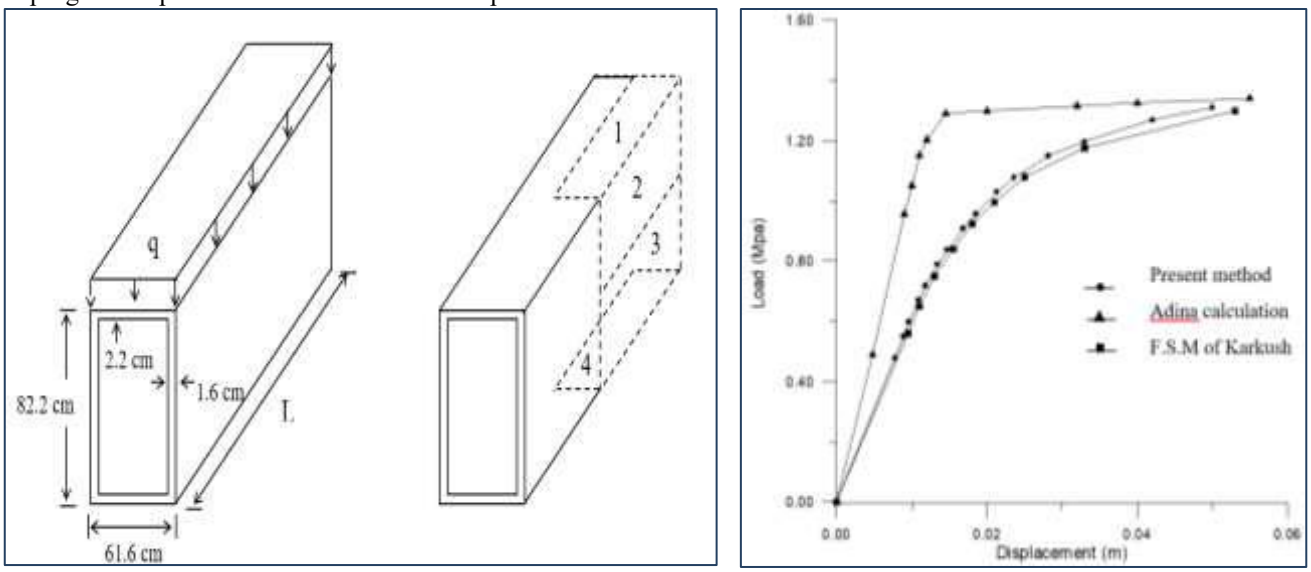

Figure 3: (a) Box beam caractrization, (b) Load-displacement curve of simply supported box beam at midspan

5.4 Closed square tank on Winkler elastic foundation

Tank properties: Storage volume = 1000 m³; Length = Width = 12.8 m; Depth = 6.1 m, Roof thickness = 0.15 m; Wall thickness = 0.23 m; Floor thickness = 0.23 m, Young's modulus: E = 28000 MPa; Poisson's ratio: ν = 1/6, Winkler modulus: k_s = 12000 kN/m³.One quarter of the tank was analyzed using 25 shell elements for each of the roof slab, walls, and floor slab. Computed bending moments were compared with Uraiby's [21]. Winkler-foundation FEM results for 20 representative element groups. Representative comparisons are presented in Table 2. The mean deviation in absolute bending moments across all 20 groups is 2.89%, confirming the accuracy of the implemented foundation stiffness matrices and the coupling between shell and foundation behaviour.

Table 2. Representative bending moments (kN·m) in the closed square tank on Winkler foundation.

Element Group	Uraiby M_x (kN·m)	Present M_x (kN·m)	Uraiby M_y (kN·m)	Present M_y (kN·m)
1	59.93	57.42	60.40	58.18
6	48.43	47.42	110.00	105.98
9	152.60	146.46	57.90	56.55
14	62.84	60.83	63.09	61.25
20	63.53	60.75	119.50	114.85

5.5 Summary of validation results

Table 3 summarizes the validation outcomes across all six benchmark problems. In all cases the differences between the present results and independent solutions remain within acceptable engineering limits, confirming the suitability of the formulation for the nonlinear analysis and optimal design of steel rectangular tanks resting on nonlinear elastic foundations.

Table 3. Summary of validation accuracy across all benchmark problems.

Example	Structural type	Comparison source	Max. error
5.1	Elastic-plastic plate	Hinton and Owen [10]	0.17% (load), 0.63% (defl.)
5.2	Hydrostatic wall	Timoshenko [35] / Uraiby [21]	7.9% / 4.3%
5.3	Elastic-plastic box beam	ADINA [11] / Karkush [16]	2.29% / 0.76%
5.4	Closed tank on foundation	Uraiby [21]	2.89% (mean)

6. Influence of Foundation Model on the Optimal Design

Material and loading properties: All optimization studies use mild steel with $E = 200{,}000$ MN/m², $\nu = 0.3$, $\sigma_y = 400$ MN/m². The stored liquid is water ($\gamma_L = 10$ kN/m³) acting as triangularly varying hydrostatic wall pressure and uniform floor pressure. A collapse load factor $\lambda_c = 1.75$ is adopted throughout. Horizontal subgrade modulus is $k_h = 0.002069$ kN/mm³ in all cases.

For the foundation model parameters: Two soil types span the practical range for sandy conditions. For the open-topped tank Kondner model: $a = 483.48$ mm³/kN and $b = 0.167$ mm²/kN. For the closed-tank polynomial study, two plate-load datasets are used: dense sand [9] and loose sand [3]. The fitted polynomial equations (P in kN/m², δ in mm) are:

Dense sand: $P = 0.443 + 79817\delta - 2.204\times10^{6}\delta^{2} + 1.941\times10^{7}\delta^{3} + 5.125\times10^{7}\delta^{4} - 9.709\times10^{8}\delta^{5}$

Loose sand: $P = 0.101 + 6277\delta - 1.302\times10^{5}\delta^{2} + 1.358\times10^{6}\delta^{3} - 5.415\times10^{6}\delta^{4}$

Dense sand shows higher initial stiffness; loose sand exhibits lower stiffness throughout the settlement range. The secant modulus k_z decreases monotonically with settlement in both cases.

6.1 Open-topped rectangular tank (100 m³)

Both the linear Winkler model and the Kondner nonlinear model converge to identical plan dimensions and shell volume (Table 4). The search trajectories in design space differ because the nonlinear foundation alters the moment redistribution pattern and effective load-factor path during optimization. However, both paths reach the same final optimum, indicating that the optimal geometry is governed primarily by the plastic design constraint and the volume objective, not by the specific form of the subgrade reaction law.

Table 4. Optimal design results for 100 m³ open-topped steel tank: Winkler vs. Kondner foundation.

Parameter	Winkler (linear)	Kondner (hyperbolic)
Optimal volume V (m³)	1.980	1.980
Length L (m)	5.42	5.42
Width W (m)	5.42	5.42
Depth D (m)	3.404	3.404
L / W	1.00	1.00
W / D	1.59	1.59
Floor thickness t_f (mm)	19.8	19.8
Wall thickness $t_l = t_w$ (mm)	19.1	19.1
No. optimization cycles	12	14

6.2 Closed rectangular tanks on polynomial foundations (100 m³ and 300 m³)

Tables 5 and 6 present optimal dimensions and thickness ratios for closed tanks. Three key findings emerge. First, the square plan (L = W) is universally optimal. Second, the optimal width-to-depth ratio is W/D ≈ 3.0–3.1 for both soil types and both tank volumes. Third, the optimal plan dimensions are identical for dense and loose sand; only shell thicknesses differ modestly.

Table 5. Optimal dimensions for closed rectangular steel tanks under polynomial soil models.

Soil type	Volume (m³)	L (m)	W (m)	D (m)	L/W	W/D
Dense sand	100	6.7	6.7	2.23	1.00	3.00
Dense sand	300	9.8	9.8	3.12	1.00	3.14
Loose sand	100	6.7	6.7	2.23	1.00	3.00
Loose sand	300	9.8	9.8	3.12	1.00	3.14

Table 6. Optimal shell thicknesses (mm) for closed rectangular steel tanks.

Soil type	Volume (m³)	Roof t_r	Wall t_l,t_w	Floor t_f	t_r : t_f : t_l
Dense sand	100	5.02	6.73	5.69	1.00 : 1.13 : 1.34
Dense sand	300	8.82	12.1	9.49	1.00 : 1.08 : 1.37
Loose sand	100	5.28	6.92	6.08	1.00 : 1.15 : 1.31
Loose sand	300	9.38	12.5	10.7	1.00 : 1.14 : 1.33

Table 7. Comparison of total optimal shell volumes between soil types.

Tank volume (m³)	V dense sand (m³)	V loose sand (m³)	Difference (%)
100	0.374	0.388	3.7%
300	1.512	1.574	4.1%

Moving from dense to loose sand increases floor thickness by 6–13%, wall thickness by 2–3%, and roof thickness by 5–7% for the 100 m³ tank; changes are similar for the 300 m³ tank. The resulting difference in total optimal shell volume is below 4% (Table 7).

6.5 Elastic vs. elastic-plastic optimal design

The 100 m³ open-topped tank was additionally optimized using linear elastic analysis with the Winkler foundation. The elastic-optimal shell volume was 2.495 m³, compared with 1.980 m³ for the elastic-plastic design—a reduction of approximately 26%. This finding is consistent with the shape factor of 1.5 for rectangular cross-sections (ratio of plastic to elastic modulus) and confirms that exploiting plastic reserves is essential for material-efficient steel tank design [22,23].

7. Discussion and Conclusions

The central finding is that the optimal tank geometry (L/W = 1.0, W/D ≈ 3:1) is insensitive to the choice of foundation model, and that the optimal shell volume differs by at most 4% between the two polynomial soil models examined. This insensitivity arises because the governing design constraint is the moment-resultant yield criterion on wall and floor cross-sections. The dominant moments in a square hydrostatic tank are driven by the hydrostatic pressure profile and the wall-floor interaction at the base joint. Foundation stiffness modifies the floor moment distribution but, within the range of practical soil stiffnesses, does not change which cross-section first reaches its plastic limit or the final collapse mechanism.

The modest sensitivity of shell thicknesses to soil type—up to 13% for the floor slab—is physically consistent: a softer foundation provides less support to the slab, transferring more bending to the floor and requiring marginally greater floor thickness to satisfy the yield constraint of Eq. (7). This is directly analogous to the behaviour documented by Loukidis and Tamiolakis [32] for mat foundations, where a non-uniform subgrade modulus alters bending moments without changing the overall structural load path.

The 26% volume saving from elastic-plastic versus elastic optimization is consistent with established plastic-analysis theory and parallels the savings documented in recent shell and plate optimization studies. This reinforces the recommendation that plastic design methods be adopted for steel liquid-storage tanks wherever ductility can be assured.

One limitation of the present study is that the soil models are calibrated against plate-load data for sandy soils under static loading. Recent literature on rectangular tank soil-structure interaction under seismic loading demonstrates that soil type and tank slenderness interact in complex ways under dynamic excitation, a topic not addressed here. Extension to seismic design, incorporating the nonlinear SSI mechanisms identified in these studies, is a natural direction for future work. The following conclusions are drawn:

- The elastic-plastic incremental FEM with eight-node flat shell elements accurately predicts the response of rectangular steel tanks on elastic foundations, validated against six independent benchmarks with mean bending-moment errors below 9%. The stress-based von Mises criterion and its equivalent moment-resultant form are consistently applied throughout.
- All three foundation models (Winkler, Kondner hyperbolic, polynomial) yield identical optimal plan dimensions and virtually identical optimal depth-to-width ratios for the tank geometries and soil conditions studied.

- The optimal plan shape is universally square (L/W = 1.0), and the optimal width-to-depth ratio is approximately W/D = 3:1, independent of soil type and tank capacity.
- Shell thicknesses show limited sensitivity to soil type: floor thickness increases by up to 13% moving from dense to loose sand, while wall and roof thicknesses change by less than 7%. The resulting change in total optimal shell volume is below 4%.
- The consistent optimal thickness ratio is t_roof : t_floor : t_wall ≈ 1.0 : 1.1 : 1.3, providing a practical design guideline independent of the foundation model.
- Elastic-plastic optimization achieves approximately 26% less shell material volume than elastic optimization for the same tank capacity, confirming the importance of nonlinear material analysis in design.

These findings justify using simpler linear (Winkler) foundation models at the preliminary optimization stage. Nonlinear foundation models are recommended for detailed design, particularly for floor slab thickness determination under soft soil conditions.

References

[1] Cheung, Y. K., & Zienkiewicz, O. C. (1965). Plates and tanks on elastic foundations: An application of finite element method. *International Journal of Solids and Structures*, *1*(4), 451–461.

[2] Cheung, Y. K., & Davies, J. D. (1967). Analysis of rectangular tanks: Use of finite element technique. *Concrete*, 169–174.

[3] Lambe, T. W., & Whitman, R. V. (1984). *Soil mechanics* (SI version, 2nd ed.). Wiley Eastern.

[4] Bowles, J. E. (1996). *Foundation analysis and design* (5th ed.). McGraw-Hill.

[5] Mourya, R. K., Kumar, S., & Rawat, A. (2023). Approaches considering non-linearity in soil-foundation-structure interaction. *Research on Engineering Structures and Materials*, *9*(3), 989–1013.

[6] Rad, S., & Ibrahim, S. K. (2021). Optimal plastic analysis and design of pile foundations under reliable conditions. *Periodica Polytechnica Civil Engineering*. Advance online publication.

[7] Kondner, R. L. (1963). Hyperbolic stress-strain response: Cohesive soils. *Journal of the Soil Mechanics and Foundations Division*, *89*(1), 115–143.

Al-Rubai, Q. K. (2001). *Large displacement elastic stability analysis of plane structures resting on non-linear Winkler foundation* [Master's thesis, University of Technology, Baghdad].

[9] Al-Khafaji, A. G. A. (2002). *Large displacement and post-buckling analysis of plane steel structures resting on elastic foundation* [Master's thesis, University of Babylon].

[10] Owen, D. R. J., & Hinton, E. (1980). *Finite elements in plasticity: Theory and practice*. Pineridge Press.

[11] Ng, [Insert Initial(s)]. et al. (1991). Finite strip method for analysis of structures with material non-linearity. *Journal of Structural Engineering*, *117*(2), 489–500.

[12] Farshid B. et al. (2024). Time domain nonlinear fluid-structure-soil interaction analysis of rectangular water storage tanks using coupled Eulerian-Lagrangian formulation. *Journal of Earthquake Engineering*, *28*(6), 1744–1768.

[13] Kumar, H., & Saha, S. K. (2022). Effects of soil-structure interaction on seismic response of fixed base and base isolated liquid storage tanks. *Journal of Earthquake Engineering*, *26*(12), 6148–6171.

[14] Chen, M., & Liu, Y. (2024). Seismic response analysis of underground large LNG tanks considering fluid-structure-soil interaction. *Applied Sciences*, *14*(11), Article 4753.

[15] Alwash, N. A. H. (1989). *Elasto-plastic and limit analysis of thick plates* [Master's thesis, University of Baghdad].

[16] Karkush, M. O. (1998). *Non-linear behavior of folded plate structures* [Master's thesis, University of Babylon].

[17] Ghali, A. (1957). *The structural analysis of circular and rectangular concrete tanks* [Doctoral dissertation, University of Leeds].

[18] Davies, J. D. (1961). The influence of support conditions on the behaviour of cylindrical concrete tanks. *Proceedings of the Institution of Civil Engineers*, *20*(3), 379–388.

[19] Husain, H. M. (1964). *The analysis of rectangular plates and cellular structures* [Doctoral dissertation, University of Leeds].

[20] Cheung, Y. K., & Davies, J. D. (1967). Bending moments in long walled tanks. *Journal of the American Concrete Institute*, *64*(10), 685–689.

[21] Uraiby, S. A. (1997). *Optimum design of reinforced concrete rectangular tank on elastic foundation* [Master's thesis, University of Baghdad].

[22] Vestergaard, J. T., Fisker, M., Overgaard, L. C. T., & Madsen, H. B. (2023). A shell element for design-oriented elasto-plastic analysis of RC wall structures using convex optimization. *Structural Concrete*, *24*(2), 2606–2622.

[23] Truong, D.-N., & Chou, J.-S. (2023). Integrating enhanced optimization with finite element analysis for designing steel structure weight under multiple constraints. *Journal of Civil Engineering and Management*, *29*(8), 757–786.

[24] Ghaemifard, S., & Ghannadiasl, A. (2024). A comparison of metaheuristic algorithms for structural optimization. *Advances in Civil Engineering*, *2024*, Article 2054173.

[25] Yuanky J. et al. (2024). Finite element analysis and improved evaluation of mechanical response in large oil storage tanks subjected to non-uniform foundation settlement. *Processes*, *12*(12), Article 2838.

[26] Meichoers, R., & Rozvany, G. (1970). Optimum design of reinforced concrete tanks. *Journal of the Engineering Mechanics Division*, *96*(6), 1093–1106.

[27] Adidam, S. R., & Subramanyam, A. V. (1982). Optimum design of reinforced concrete water tanks. *Journal of the Structural Division*, *108*(6), 1219–1231.

[28] Abdul-Hussain, K. (1985). *Optimum design of structures* [Master's thesis, University of Technology, Baghdad].

[29] Therendran, V., & Thambiratnam, D. P. (1986). Minimum weight design of cylindrical water tanks. *International Journal for Numerical Methods in Engineering*, *23*(9), 1679–1691.

[30] Al-Ne'aimi, A. A. H., & Al-Sabah, A. I. (1988). Optimum design of R/C cylindrical tanks with tapered walls. *Proceedings of the 2nd Iraqi Engineering Conference*, University of Mosul.
[31] Al-Ne'aimi, A. A. H., & Al-Sabah, A. I. (1989). Minimum cost design of underground R/C cylindrical tanks. *Proceedings of the 5th Iraqi Engineering Conference*, *4*.
[32] Loukidis, D., & Tamiolakis, G. P. (2017). Spatial distribution of Winkler spring stiffness for rectangular mat foundation analysis. *Engineering Structures*, *153*, 443–459.
[33] Jing, W., Wang, S., & Shen, J. (2024). Seismic control of adjacent liquid storage tanks based on vibration barrier considering structure-soil-structure interaction. *Journal of Earthquake Engineering*, *28*(10), 2924–2946.
[34] Bunday, B. D. (1984). *Basic optimization methods*. Edward Arnold.
[35] Timoshenko, S., & Woinowsky-Krieger, S. (1959). *Theory of plates and shells*. McGraw-Hill.
[36] Save, M. A., & Massonnet, C. E. (1972). *Plastic analysis and design of plates, shells and disks*. North-Holland.
[37] Moy, S. S. J. (1985). *Plastic methods for steel and concrete structures*. Macmillan.